J. Plasma Phys. (2020), *vol.* 86, 905860315 © The Author(s), 2020.
Published by Cambridge University Press
doi:10.1017/S0022377820000549

Suppression of turbulence in the drift-resistive plasma where zonal flow changes direction

Chang-Bae Kim†

Physics Department and Research Institute for Origin of Matter and Evolution of Galaxies, Soongsil University, Seoul 06978, Korea

(Received 4 September 2019; revised 13 May 2020; accepted 13 May 2020)

The edge region of quasi-adiabatic plasma is pedagogically simulated by the dynamics between the electric potential φ and the electron density n whose equilibrium density gradient is negative and held fixed. The zonal flow (ZF) V is either enforced sinusoidally or generated self-consistently from the turbulence. Cross-phase δ between φ and n, which is important in the determination of the turbulence level and the transport, is strongly influenced by the ZF. In the region near $V = 0$, δ becomes negative due to the large gradient of the ZF. It is found that the instabilities are quenched there, and the fluctuations decay. The ZF thus works as a transport barrier in the region where the ZF changes direction with large gradient.

Key words: fusion plasma, plasma nonlinear phenomena

1. Introduction

Zonal flows (ZFs) in fusion plasmas modify the nature of the turbulence and the transport (Diamond *et al.* 2005; Fujisawa 2009). Near the plasma edge, the formation of the transport barrier that improves the fusion plasma confinement, consequently called the H-mode, is strongly tied to the presence of the ZF (Wagner *et al.* 1982; Hillesheim *et al.* 2016; Wagner 2018). Turbulence feeds the energy to the ZF through the Reynolds stress (Biglari, Diamond & Terry 1990; Rosenbluth & Hinton 1998; Horton 1999; Krommes & Kim 2000; Diamond *et al.* 2005). It is argued that a meso-scopically non-uniform ZF hampers the turbulent transport by the eddies at the micro-scale if the ZF shearing action on the eddies is faster than the turbulent mixing rate (Shaing & Crume 1989; Biglari *et al.* 1990; Burrell 1999). The ZF may also efficiently dissipate the energy of the unstable modes by working as a catalyst in the transfer of energy to the stable modes through the three-wave interactions (Makwana *et al.* 2014). Such a scenario of ZF-mediated energy redistribution qualitatively explains the gross features of the observed transport of H-mode plasmas in experiments and numerical simulations. The level of the plasma fluctuation is of major concern in this argument, however, and the phase relations between the fluctuations are mostly overlooked. The transport of the plasma particles and the energy by the $\boldsymbol{E} \times \boldsymbol{B}$ drift, where E is the electric field and B the magnetic field, are directly dependent on the cross-phases. The radially outward transport works

† Email address for correspondence: cbkim@ssu.ac.kr

https://doi.org/10.1017/S0022377820000549 Published online by Cambridge University Press

to drive up the fluctuation level in the drift-wave turbulence. The importance of the cross-phase has been noted by Kobayashi *et al.* (2017) and experiments have measured the cross-phase and have drawn comparisons with the numerical simulations in the tokamak geometry (Tynan, Fujisawa & McKee 2009; White *et al.* 2010; Shchepetov, Kholnov & Vasil'kov 2013; Freethy *et al.* 2018; Guttenfelder *et al.* 2019). Roles of the cross-phases have been studied in simple models where sheared flows are present (Naulin & Spatschek 1997; Carmargo, Tippett & Caldas 1998; Terry 2000; Terry, Newman & Ware 2001; Figarella *et al.* 2003; Schaffner *et al.* 2012; Birkenmeier *et al.* 2013).

Recent work by Kim, Min & An (2019*b*) found that the cross-phase between the electric potential and the electron density fluctuations plays a critical role in the saturated state of the drift-resistive turbulence because a non-uniform ZF strongly modifies the cross-phase. It was shown that the turbulence is localized where a sinusoidally varying ZF is a peak and that the zonal fields tend to lower the cross-phase at the peaks of the turbulence. The present work intends to explain the localization as a result of the plasma being stabilized through the inward particle advection and the resistive loss around the region of the ZF changing direction. Particle flux across the background density profile, if it is positive (radially outward), is a major source of free energy for the electron density fluctuations. Negative cross-phase corresponds to negative flux. The fluid of the plasma in the perpendicular plane to the magnetic field, meanwhile, is mostly powered by the resistive motion of the electrons in the parallel direction. Since the resistive electric current is proportional to the sum of the electric force and the pressure gradient (or density gradient in the case of constant temperature), the resistive Joule heating depends on the relative level as well as the cross-phase between the potential and density fluctuations. Using standard normalizations, if the density level is lower than the electric potential, ohmic loss leads to the loss of the $\boldsymbol{E} \times \boldsymbol{B}$ kinetic energy irrespective of the cross-phase. Thus, a negative cross-phase drives down the density fluctuation and the kinetic energy decays when the density level is below the potential. Following a brief encounter with the modified Hasegawa–Wakatani model we present the numerical results and the analyses for two cases of the ZF, one being sinusoidally forced and the other generated inherently. We then conclude.

2. Modified Hasegawa–Wakatani model

Hasegawa–Wakatani model (HWM) describes the dynamics of the fluctuations of the electrostatic potential φ and the electron density n in the x–y plane perpendicular to the magnetic field (Hasegawa & Wakatani 1983). The equilibrium density gradient is held fixed in the HWM. One of the two equations in the model enforces the steady current and the other is the electron continuity. The electric current flows in the direction perpendicular to the magnetic field due to the ion polarization drifts and in the parallel direction due to the resistive motion of the electron fluid. The electron resistive current is proportional to the sum of the electric force and the density gradient with the coefficient being the conductivity σ. Typical units of the HWM are ρ_s for the spatial scale, L_n/c_s for the time, $(T_e\rho_s/eL_n)$ and $(n_0\rho_s/L_n)$ for φ and n, respectively, where L_n is the length scale of the equilibrium density, $c_s = \sqrt{T_e/M_i}$ and $\rho_s = c_s/\Omega_i$. The electron temperature is T_e, the electron charge e, the ion mass M_i, the ion gyro-frequency Ω_i and the background density n_0.

The modified version of the HWM (mHWM) excludes the resistive damping of the zonal mode which changes only along the direction of the background density gradient

https://doi.org/10.1017/S0022377820000549 Published online by Cambridge University Press

(Numata, Ball & Dewar 2007). In dimensionless form the mHWM is

$$\partial_t \omega + [\varphi, \omega] = \alpha(\tilde{\varphi} - \tilde{n}) - \nu \nabla_\perp^4 \omega, \tag{2.1}$$

$$\partial_t n + [\varphi, n] = -\partial_y \varphi + \alpha(\tilde{\varphi} - \tilde{n}) - \nu \nabla_\perp^4 n, \tag{2.2}$$

where $\omega = \nabla_\perp^2 \varphi$ is the vorticity, $\tilde{\varphi} = \varphi - \bar{\varphi}$ and $\tilde{n} = n - \bar{n}$ are the non-zonal parts. The zonal components $\bar{\varphi}$ and $\bar{n}$ are independent of y because they are the averages of the corresponding fluctuations over y. With the units, the gradient of the equilibrium density n_0 is fixed to be $\nabla n_0 = -\hat{\boldsymbol{x}}$. On the left-hand sides of (2.1) and (2.2) the Poisson brackets, e.g. $[\varphi, \omega] = (\hat{z} \times \boldsymbol{\nabla}_\perp \varphi) \cdot \boldsymbol{\nabla} \omega$, denote the $\boldsymbol{E} \times \boldsymbol{B}$ advection. The electron diamagnetic drift is along y, and the magnetic field is along z. The terms $\alpha(\tilde{\varphi} - \tilde{n})$ in (2.1) and (2.2) come from the divergence of the parallel resistive current and the parallel compression, respectively. Variation along the magnetic-field direction is parametrized by α that is proportional to σ and inversely proportional to the square of a typical length scale along z. Since σ increases with the electron temperature T_e, the parameter α is roughly larger for higher T_e. Electrons are almost adiabatic if $\alpha > 1$. Artificial hyper-diffusion of order four is introduced in order to cut off the smaller-scale non-zonal fluctuations with the coefficient ν. For the zonal fields artificial diffusion of order 2 with different coefficient $\bar{\nu}$ is used.

Evolution of the non-zonal fields is reduced from (2.1) and (2.2)

$$(\partial_t + \bar{V}\partial_y + \nu \nabla_\perp^4)\tilde{\omega} + [\tilde{\varphi}, \tilde{\omega}] - \bar{\Pi}'' = \bar{V}'' \partial_y \tilde{\varphi} + \alpha(\tilde{\varphi} - \tilde{n}), \tag{2.3}$$

$$(\partial_t + \bar{V}\partial_y + \nu \nabla_\perp^4)\tilde{n} + [\tilde{\varphi}, \tilde{n}] - \bar{\Gamma}' = (-1 + \bar{n}')\partial_y \tilde{\varphi} + \alpha(\tilde{\varphi} - \tilde{n}), \tag{2.4}$$

where $\bar{V} = \partial_x \bar{\varphi}$ is the zonal flow, the Reynolds stress $\bar{\Pi} = \overline{\tilde{v}_x \tilde{v}_y} = -\overline{\partial_x \tilde{\varphi} \partial_y \tilde{\varphi}}$ and the particle transport $\bar{\Gamma} = \overline{\tilde{n} \tilde{v}_x} = -\overline{\tilde{n} \partial_y \tilde{\varphi}}$. It is convenient to express (2.3) and (2.4) in the Fourier space in the y direction. The Fourier modes of $\tilde{\varphi}(x, y, t)$ and $\tilde{n}(x, y, t)$ with the wavenumber k are $\tilde{\varphi}_k(x, t) = |\tilde{\varphi}_k| \mathrm{e}^{\mathrm{i}\theta_k^\varphi}$ and $\tilde{n}_k(x, t) = |\tilde{n}_k| \mathrm{e}^{\mathrm{i}\theta_k^n}$, respectively. Upon multiplying (2.3) and (2.4) in the Fourier space by $-\tilde{\varphi}_k^*$ and $\tilde{n}_k^*$, respectively, and taking the real parts, one obtains the evolution equations for the kinetic energy $K_k = \frac{1}{2}|\nabla_\perp \tilde{\varphi}_k|^2$ and the particle-density energy $P_k = \frac{1}{2}|\tilde{n}_k|^2$

$$\partial_t K_k = \bar{V} \Pi_k' - \alpha |\tilde{\varphi}_k|^2 (1 - \beta_k \cos \delta_k) + \mathrm{Re}\{\tilde{\varphi}_k^* [\tilde{\varphi}, \tilde{\omega}]_k\} - (\mathrm{HL}) + S, \tag{2.5}$$

$$\partial_t P_k = (1 - \bar{n}') \Gamma_k + \alpha |\tilde{\varphi}_k|^2 \beta_k (\cos \delta_k - \beta_k) - \mathrm{Re}\{\tilde{n}_k^* [\tilde{\varphi}, \tilde{n}]_k\} - (\mathrm{HL}), \tag{2.6}$$

where $\beta_k = |\tilde{n}_k| / |\tilde{\varphi}_k|$ is the ratio of the amplitudes and $\delta_k = \theta_k^\varphi - \theta_k^n$ the cross-phase, $S = \partial_x \mathrm{Re}(\tilde{\varphi}_k^* \partial_x \partial_t \tilde{\varphi}_k)$ the surface term and HL the hyper-dissipation. The particle transport is $\Gamma_k = k |\tilde{\varphi}_k|^2 \beta_k \sin \delta_k$ and the Reynolds stress $\Pi_k = -k \mathrm{Im}(\tilde{\varphi}_k^* \partial_x \tilde{\varphi}_k)$. The primes mean derivatives with respect to x. One notes that the energy-exchange term between the non-zonal fluctuation and the zonal flow in (2.5) is the sum of two terms, $\bar{V} \Pi_k' = -\bar{V}' \Pi_k + \partial_x (\bar{V} \Pi_k)$, the former of which is usually cited as the zonal-flow shearing on the fluctuating eddies.

In the linear phase, after the plasma is disturbed by an infinitesimally small perturbation, the plasma may become unstable. Since K_k is driven by $-\alpha |\tilde{\varphi}_k|^2 (1 - \beta_k \cos \delta_k)$ in (2.5), for a certain mode $\tilde{\varphi}_k$ to grow in time β_k is necessarily larger than one when all fields are sufficiently weak. For such an unstable mode the resistive response works as a loss of power $-\alpha |\tilde{\varphi}_k|^2 (\beta_k - \cos \delta_k)$ to P_k. Since the particle transport Γ_k powers the growth of $\tilde{n}_k$ in (2.6), the cross-phase needs to be positive, $\delta_k > 0$, for the growth of $\tilde{n}_k$ in order to keep $\beta_k > 1$. On the other hand, if $\beta_k < \cos \delta_k$

https://doi.org/10.1017/S0022377820000549 Published online by Cambridge University Press

the perturbation $\tilde{\varphi}_k$ decreases in time. In order to keep $\beta_k < \cos\delta_k\ \tilde{n}$ the perturbation cannot increase in time. It is thus necessary that Γ_k be negative, that is, $\delta_k < 0$. For a mode of $\cos\delta_k < \beta_k < 1$, which is a very small window for a highly adiabatic electron plasma, it is possible that δ_k is positive and the mode is decaying. Energy is transferred to other modes by nonlinear interactions and may be used to excite the zonal fields.

Upon taking the zonal parts of (2.1) and (2.2) one obtains the evolution equations of the zonal fields

$$\partial_t \bar{V} = -\partial_x(\bar{\Pi} + \bar{\nu}\partial_x^3 \bar{V}), \tag{2.7}$$

$$\partial_t \bar{n} = -\partial_x(\bar{\Gamma} + \bar{\nu}\partial_x^3 \bar{n}). \tag{2.8}$$

After multiplying (2.7) by $\bar{V}$ and (2.8) by $\bar{n}$ one finds that the zonal kinetic energy $\bar{V}^2/2$ is driven by the non-zonal turbulence $-\bar{V}\bar{\Pi}'$ and that the zonal-density energy $\bar{n}^2/2$ by $-\bar{n}\bar{\Gamma}'$. Since $\bar{\Pi} = \sum_k \Pi_k$, the exchange of the kinetic energy between the zonal and non-zonal parts is exactly balanced out.

For the purpose of studying the cross-phase it is better to reduce (2.3) for $\tilde{\varphi}$. After the inverse of the Laplacian $\nabla_\perp^{-2}$ is applied, equation (2.3) changes to

$$(\partial_t + \bar{V}\partial_y + \nu\nabla_\perp^4)\tilde{\varphi} + \nabla_\perp^{-2}[\tilde{\varphi}, \tilde{\omega}] - \bar{\Pi} = 2\nabla_\perp^{-2}\partial_x(\bar{V}'\partial_y\tilde{\varphi}) + \alpha\nabla_\perp^{-2}(\tilde{\varphi} - \tilde{n}). \tag{2.9}$$

After the Fourier transformation in y one obtains the equation of δ_k (Kim, An & Min 2019*a*)

$$\partial_t \delta_k = \mathcal{H}_k + \mathcal{Z}_k + \mathcal{N}_k, \tag{2.10}$$

where $\mathcal{H}_k$ is homogeneous and explicitly independent of the zonal fields,

$$\mathcal{H}_k = k\frac{\mathrm{Re}(\tilde{n}_k^*\tilde{\varphi}_k)}{|\tilde{n}_k|^2} + \alpha\left(\frac{\mathrm{Im}\{\tilde{\varphi}_k^*[\nabla_\perp^{-2}(\tilde{\varphi} - \tilde{n})]_k\}}{|\tilde{\varphi}_k|^2} - \frac{\mathrm{Im}(\tilde{n}_k^*\tilde{\varphi}_k)}{|\tilde{n}_k|^2}\right), \tag{2.11}$$

$\mathcal{Z}_k$ explicitly depends on $\bar{V}$ and $\bar{n}'$,

$$\mathcal{Z}_k = -k\bar{n}'\frac{\mathrm{Re}(\tilde{n}_k^*\tilde{\varphi}_k)}{|\tilde{n}_k|^2} + 2\frac{\mathrm{Im}\{\tilde{\varphi}_k^*[\nabla_\perp^{-2}\partial_x(\bar{V}'\partial_y\tilde{\varphi})]_k\}}{|\tilde{\varphi}_k|^2}, \tag{2.12}$$

and the non-zonal part

$$\mathcal{N}_k = -\frac{\mathrm{Im}\{\tilde{\varphi}_k^*\nabla_\perp^{-2}[\tilde{\varphi}, \tilde{\omega}]_k\}}{|\tilde{\varphi}_k|^2} + \frac{\mathrm{Im}\{\tilde{n}_k^*[\tilde{\varphi}, \tilde{n}]_k\}}{|\tilde{n}_k|^2}. \tag{2.13}$$

By introducing δ_{0k} as the solution of $\mathcal{H}_k(\delta_{0k}) = 0$ one may separate $\delta_k = \delta_{0k} + \delta_{1k}$ so that the explicit dependence on the zonal fields is collected in δ_{1k}

$$\delta_{0k} = \tan^{-1}\left[\frac{k}{\alpha}\left(1 + \frac{\beta_k^2}{k_\perp^2}\right)^{-1}\right], \tag{2.14}$$

where $k_\perp = |\nabla_\perp\tilde{\varphi}_k|/|\tilde{\varphi}_k|$ is the typical inverse scale of $\tilde{\varphi}_k$. In the case of a near-adiabatic steady state, equation (2.10) leads to

$$\sin\delta_{1k} \approx \beta_k\left[\sqrt{k^2 + \alpha^2\left(1 + \frac{\beta_k^2}{k_\perp^2}\right)^2}\right]^{-1}(\mathcal{Z}_k + \mathcal{N}_k). \tag{2.15}$$

https://doi.org/10.1017/S0022377820000549 Published online by Cambridge University Press

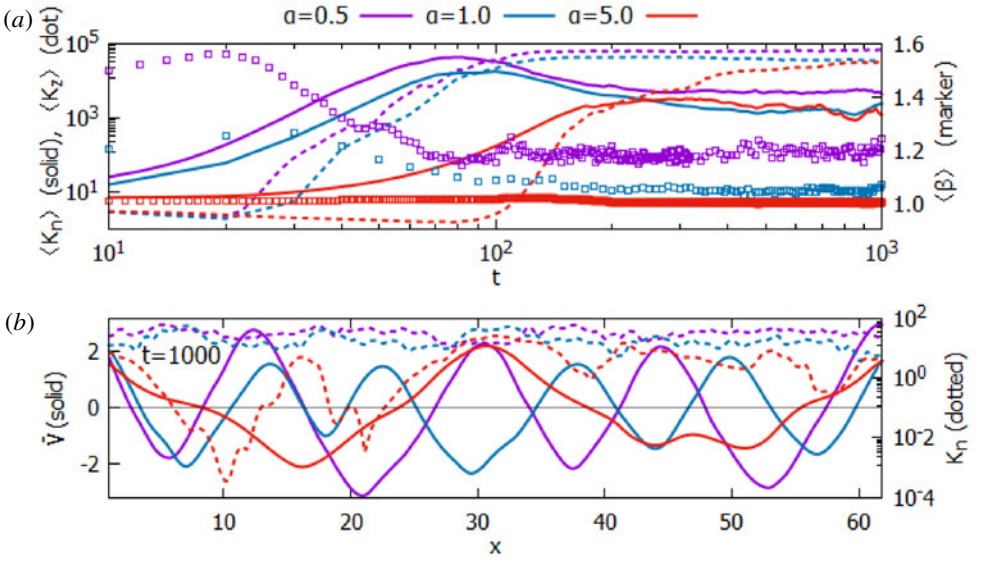


FIGURE 1. Evolution toward quasi-steady state and the profiles of the zonal field and the turbulence for $\alpha = 0.5$, 1.0 and 5.0. (*a*) Change in time of the zonal and non-zonal kinetic energies, $\langle K_z \rangle$ (dotted line) and $\langle K_n \rangle$ (solid line), and $\langle \beta \rangle$ (with markers) which is the square root of the ratio between the non-zonal particle density and the potential energies. (*b*) The zonal flow $\bar{V}$ and the non-zonal kinetic energy K_n summed over the y axis.

3. Results and discussion

Equations (2.1) and (2.2) are numerically integrated in time on the BOUT++ platform (Dudson *et al.* 2009). A square domain of length $L = 20\pi$ is turned into the set of 256^2 equally spaced grid points with the spacing $\Delta x = \Delta y \approx 0.25$. For the differentials in space, a fourth-order finite-difference scheme is used and the advance in time is made possible by PVODE with adaptive time stepping. In order to treat the Poisson brackets, the Arakawa scheme (Arakawa 1966) is adopted. The simulation starts from the initial state of zero density perturbation and non-zero pseudo-random vorticity $\omega(x, y) = 10^{-2} \sum_{j,k=1}^{15} \cos(2j\pi x/L + \theta_j) \cos(2k\pi y/L + \theta_k)$ with random phase constants θ. The fluctuations are enforced to satisfy the periodic boundary conditions. We consider the cases of a near-adiabatic electron response so that the parameter α in (2.1) and (2.2) is set to 5 if not stated otherwise. The coefficient of the fourth-order hyper-diffusion is $\nu = 1 \times 10^{-4}$ for the non-zonal fields. The diffusion coefficient of the zonal fields is $\bar{\nu} = 1 \times 10^{-2}$. Zonal flow is self-consistently generated from the non-zonal fields by the dynamics of (2.1) and (2.2). The simulation result for the case of $\alpha = 5.0$ is most interesting so that this result is mainly highlighted and compared to the case where the zonal flow is specified to be a sinusoidal profile.

Gross features of the simulations with $\alpha = 0.5$, 1.0 and 5.0 are plotted in figure 1. In the upper part the evolutions toward quasi-steady state are shown of the kinetic energies of the zonal $\langle K_z \rangle = \int \mathrm{d}x\,\mathrm{d}y \bar{V}(x)^2/2$ and the non-zonal $\langle K_n \rangle = \int \mathrm{d}x\,\mathrm{d}y |\nabla_\perp \tilde{\varphi}|^2/2$ flows and $\langle \beta \rangle = \sqrt{\int \mathrm{d}x\,\mathrm{d}y \tilde{n}^2 / \int \mathrm{d}x\,\mathrm{d}y \tilde{\varphi}^2}$, which represents a global measure for the adiabaticity. It is found that the non-zonal fluctuations grow initially and the zonal flows become excited out of the non-zonal turbulence. For smaller α, the linear growth of the non-zonal fluctuations is faster, the zonal flows appear earlier and the

https://doi.org/10.1017/S0022377820000549 Published online by Cambridge University Press

fluctuations saturate sooner. By the time $t = 10^3$, $\langle K_z \rangle$ becomes greater than $\langle K_n \rangle$ by more than an order of magnitude and both of them saturate at higher levels for smaller α. $\langle \beta \rangle$ becomes saturated at larger value for smaller α. This is because the main destabilizing factor in the HWM is the adiabaticity between $\tilde{\varphi}$ and $\tilde{n}$, which is inversely related to α. In the lower part of figure 1 the profiles of the zonal flow and the distributions of the non-zonal kinetic energy $K_n(x) = \int \mathrm{d}y |\nabla_\perp \tilde{\varphi}|^2/2$ are plotted for the same three α at $t = 10^3$.

Peak speed of the zonal flows is around 2 and $\bar{V}$ values vary quasi-periodically across x with a different periodicity between $L_x/2$ and $L_x/5$ depending on α. This is because most non-zonal energy is carried by the large-scale (wavenumber $k \ll 1$ in x) fluctuations. For $\alpha = 5.0$ zonal flow mostly extracts energy from the period-two non-zonal fluctuations. Right portion of $\bar{V}$ of $\alpha = 5.0$, by the way, needs more time to saturate (see figure 3). A striking difference between the less adiabatic cases of $\alpha = 0.5$ and 1.0 and the highly adiabatic case of $\alpha = 5.0$ is the turbulence distribution. In the former cases the turbulence is widespread, not particularly localized where $|\bar{V}|$ is large and its peaks are not prominent. For $\alpha = 5.0$, in contrast, the non-zonal fluctuations are well separated, being localized where $\bar{V}$ is fast at $x \approx 16$ and 30. Incidentally, the right part of $\bar{V}$ around $x \approx 47$ has not yet reached the stationary state by $t = 10^3$. Since such localization is unique and interesting, further analysis of the results in the case of $\alpha = 5.0$ continues.

Such localization by the zonal flow has been reported in the presence of the zonal flow being forced externally, instead of being self-consistently derived from the mHWE (Kim *et al.* 2019*b*). A sinusoidally varying zonal flow $\bar{V}(x) = 2\cos(4\pi x/L)$ is enforced and the non-zonal fluctuations are computed accordingly. The zonal density, in contrast, is allowed to evolve based on (2.1) and (2.2). Forced ZF model takes advantage of analytical understandings of the linear state in the presence of the zonal flow. It was reported that the linear eigenmodes are localized around a positive peak of $\bar{V}$ (Kim, Min & An 2018). After an initial exponential growth of the perturbation, the level of the non-zonal fluctuations increases, the nonlinear $\boldsymbol{E} \times \boldsymbol{B}$ advection terms in (2.3) and (2.4) become dominant and the growth of the zonal density follows (Kim *et al.* 2019*b*). As a result, the growth of the fluctuations slows down and by the time $t = 10^3$ they saturate.

Results of two simulations with ZF either being forced or self-consistent in the case of $\alpha = 5.0$ are compared in figure 2. Spectral distributions of $\tilde{\varphi}_k(x)$, $\sin \delta_k(x)$ and $\beta_k(x)$ around $t = 10^3$ for the forced case and around $t = 2 \times 10^3$ for the self-consistent case are shown in the figure. In panel (*a*,*b*) it is shown that, in both cases, the fluctuations are well separated and are localized where $\bar{V}$ (black solid line in the figure) is a positive (along the electron diamagnetic drift) peak. Similarity between the two cases stops, however, where $\bar{V}$ is a negative peak: turbulence is localized in the relatively narrow region in the dynamically consistent case while it is absolutely weak in the forced case. This is because, in the self-consistent case, fast ZF needs strong turbulence as an energy supplier in contrast to the forced fast ZF. In the steady state of the self-consistent turbulence the Reynolds stress supports the zonal flow by (2.7), $\bar{\Pi}' = -\bar{\nu}\partial_x^4 \bar{V}$. Since the supplied power by the non-zonal fluctuations is $-\bar{V}\bar{\Pi}'$, $\bar{\Pi}'$ needs to be positive and peaked where $\bar{V}$ is a negative local peak. As a result, the zonal-density gradient $\bar{n}'$ (black dotted line in the figure) is almost zero in the forced case (2.8) whereas it develops a positive peak in the self-consistent case, which will be explained in the next paragraph. In the forced case, contrary to the conventional wisdom, the turbulence level at a negative peak of $\bar{V}$ where $\bar{V}' = 0$ is weaker than where $\bar{V}'$ is large ($x = 7.5\pi$ and 12.5π). This is because the zonal flow is already

https://doi.org/10.1017/S0022377820000549 Published online by Cambridge University Press

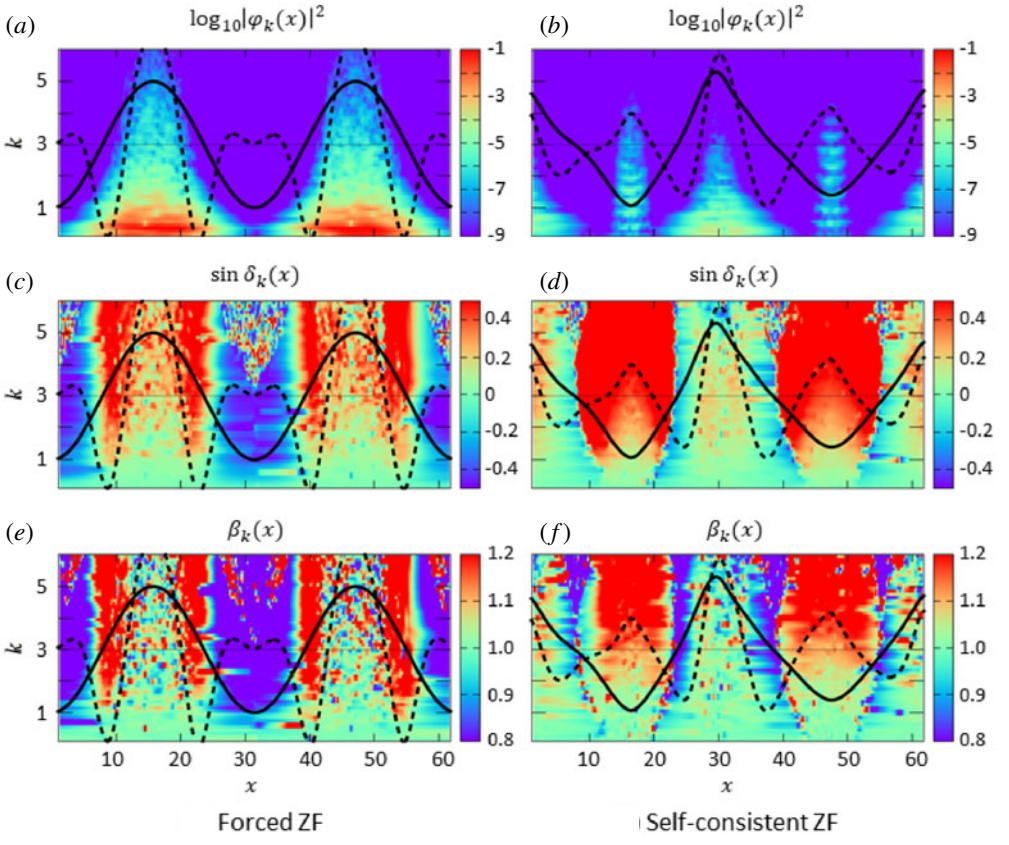


FIGURE 2. Self-consistent non-zonal turbulence of $\alpha = 5$ (b,d,f) is compared to the case of externally forced zonal flow $\bar{V} = -2\cos(x/5)$ (a,c,e) at a quasi-steady state around $t = 2 \times 10^3$. From panel (a,b): colour maps in the x–k plane of the turbulence distribution $|\tilde{\varphi}_k|^2$, the sine of the cross-phase $\sin\delta_k$ and the ratio between the particle density and the potential $\beta_k = |\tilde{n}_k|/|\tilde{\varphi}_k|$. Superimposed are the zonal flow (black solid line), in the scale between -3 and 3, and the zonal-density gradient (black dotted line) in the scale between -0.6 and 0.6.

set up when the plasma equilibrium is disturbed. Linear study finds the perturbation decays fastest where $\bar{V}$ is a negative maximum (Kim *et al.* 2018). In the nonlinear phase, therefore, the nonlinear effect is not large and turbulence is kept small even in the saturated state if $\bar{V}$ is large enough (Kim *et al.* 2019*b*). The energy spectrum depends on the sign of $\bar{V}$ at the peak locations: where positive around $x = 30$ the fluctuations of small $k < 1$ are energetic whereas at negative peaks the energy is spread over the fluctuations with wider range of k up to around 2. Spectral distributions are more closely examined below. In figure 2(c,d) δ_k of the energetic fluctuations are small and positive where $\bar{V}$ is a positive peak for both cases of forced and self-consistent ZFs. Around where $\bar{V}$ is a negative peak, δ_k values in the self-consistent case are also positive so that the plasma needs to be unstable to balance the damping. In the narrow layer where $|\tilde{\varphi}_k|^2$ is negligibly small, δ_k are negative. It is consistent with the fact that the fluctuation is weak because positive δ_k drives the density fluctuations unstable in (2.6). In the forced case, the region of weak fluctuations where $\bar{V}$ is a negative peak

https://doi.org/10.1017/S0022377820000549 Published online by Cambridge University Press

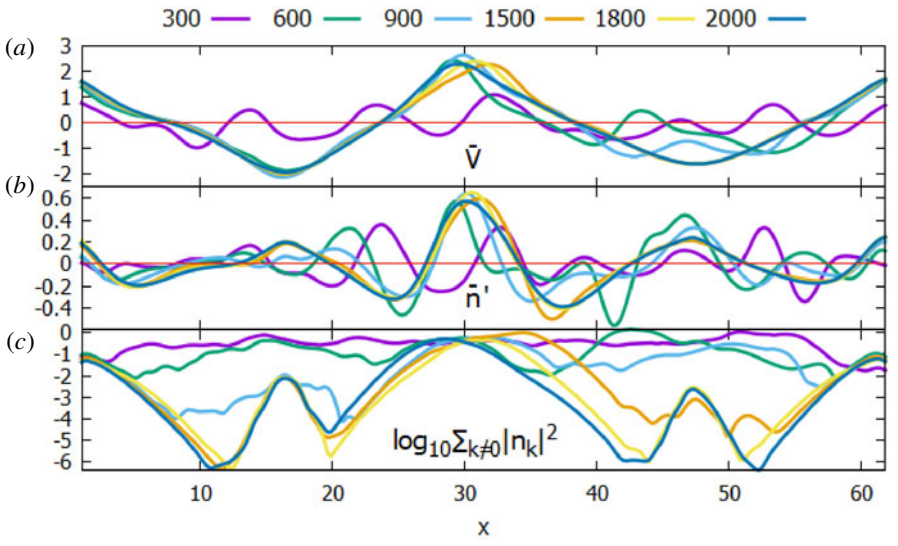


FIGURE 3. The profiles of the zonal flow $\bar{V}$ (*a*), the zonal-density gradient $\bar{n}'$ (*b*) and the non-zonal density fluctuations $\sum_k |\tilde{n}_k|^2$ (*c*) at representative times $t = 3 \times 10^2$, 6×10^2, 9×10^2, 1.5×10^3, 1.8×10^3 and 2×10^3.

accordingly corresponds to negative δ_k. Since $\tilde{\varphi}$ is driven unstable if $\beta_k > 1$ (2.5), one finds in figure 2(*e*,*f*) that $\beta_k < 1$ in the regions of weak turbulence for both cases.

Turbulence in the case of a dynamically generated ZF is further analysed for $\alpha = 5.0$ in the following. Figure 3 shows the profiles of $\bar{V}$ (*a*), $\bar{n}'$ (*b*) and the non-zonal-density fluctuations $\sum_k |\tilde{n}_k|^2$ (*c*) at representative times $t = 3 \times 10^2$, 6×10^2, 9×10^2, 1.5×10^3, 1.8×10^3 and 2×10^3. Part of $\bar{V}$ profile around $x = 16$ becomes quasi-stationary by the time $t = 600$ whereas the right part of the profile around $x = 47$ does not reach quasi-steady state until $t = 1500$ while the middle portion around $x = 30$ keeps oscillating in time. Similarly to $\bar{V}$, $\bar{n}'$ and $\sum_{k\neq 0} |\tilde{n}_k|^2$ evolve in time as the right part settles down later, lagging the left, while the central region oscillates. It is interesting to note that there are twice as many peaks of $\bar{n}'$ as of $\bar{V}$ and, unlike $\bar{V}$, only the positive peaks of $\bar{n}'$ are coincident with the locations of the localized turbulence. In the steady state, particle transport supports the zonal-density profile from (2.8), $\bar{\Gamma} = -\bar{\nu}\partial_x^3 \bar{n}$. Where $\bar{\Gamma}$ is positive and narrowly peaked symmetrically around x_0, $\bar{n}'''$ is negatively peaked and $\bar{n}''$ crosses zero from positive to negative at x_0. Therefore $\bar{n}'$ is positively peaked at x_0. If $\bar{n}$ is diffusively dissipated, $\nu_2 \bar{n}''$, instead of $-\bar{\nu}\partial_x^4 \bar{n}$, the balance would be $\bar{\Gamma} = \nu_2 \bar{n}'$ and the turbulence would be still strong at the positive peaks of $\bar{n}'$. Non-zonal fluctuations show an interesting feature during relaxation. Both in the left and right parts, depending on the locations, the fluctuations decay in time with different rates: in the regions of peak zonal flow they decrease slower and reach a stationary state sooner. Since the fluctuations in the narrow regions surrounding the peaks of $\bar{V}$ keep declining before saturation, fluctuations are trapped in the regions around the peaks of $\bar{V}$ and they are separated from each other.

Plots in figure 4 represent the degree of difference between $\tilde{\varphi}$ and $\tilde{n}$, which is the cause of the instability. The profiles of $\sin\delta(x) \doteq \overline{\tilde{n}\tilde{v}_x}/\sqrt{\overline{\tilde{n}^2}\,\overline{\tilde{v}_x^2}}$ and $\beta(x) \doteq \sqrt{\overline{\tilde{n}^2}}/\sqrt{\overline{\tilde{\varphi}^2}}$, where over-lines means summations over the y axis, are shown in figure 4 at times $t = 6 \times 10^2$, 8×10^2, $t = 1.3 \times 10^3$ and 2×10^3. Also included in the figures are the zonal

https://doi.org/10.1017/S0022377820000549 Published online by Cambridge University Press

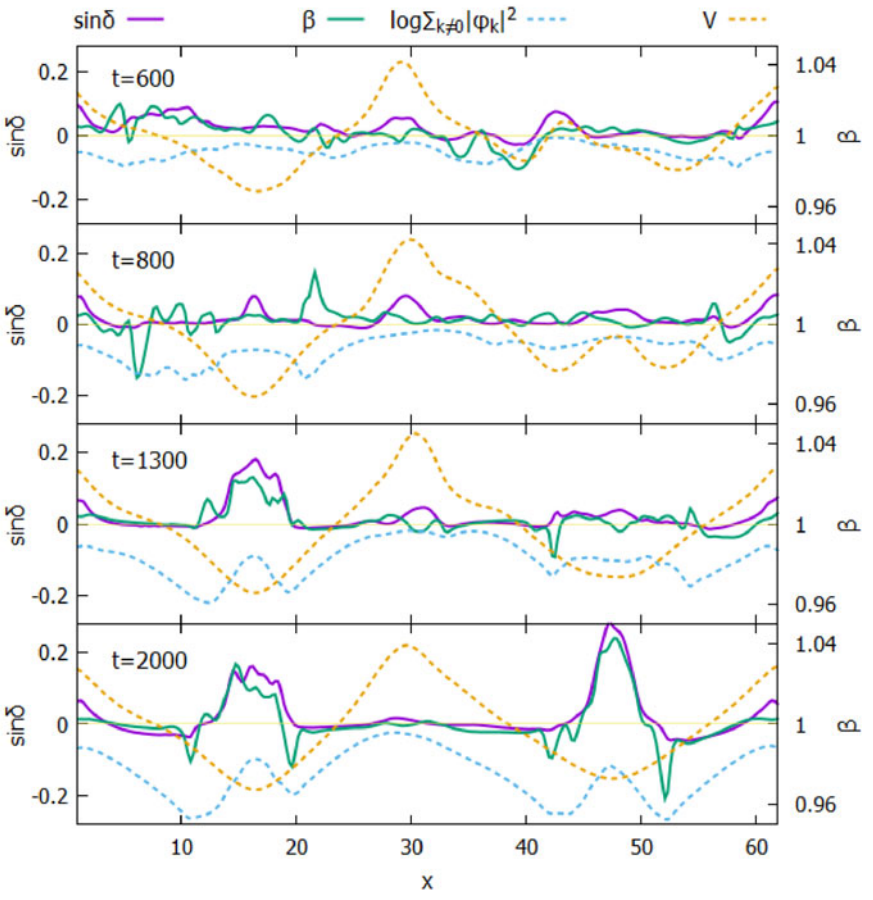


FIGURE 4. The profiles of $\sin\delta(x) \doteq \overline{\tilde{n}\tilde{v}_x}/\sqrt{\overline{\tilde{n}^2}\,\overline{\tilde{v}_x^2}}$ and $\beta(x) \doteq \sqrt{\overline{\tilde{n}^2}}/\sqrt{\overline{\tilde{\varphi}^2}}$ at representative times $t = 6\times10^2$, 8×10^2, 1.3×10^3 and 2×10^3. Superimposed are the zonal flow $\bar{V}$ (yellow dotted line) and the fluctuation distribution (blue dotted line) respectively scaled to fit in the frames.

flow $\bar{V}$ (yellow dotted line) and the fluctuation distribution (blue dotted line) that are properly rescaled to fit. By $t=10^3$ both $\sin\delta$ and β become pronounced as high as 0.2 and 1.04 respectively around $x=16$, where $\bar{V}$ is negative and fast and the turbulence is locally peaked, and stay almost unchanged afterwards. Later, by $t=1.6\times10^3$, they also become locally large around $x=47$ where $\bar{V}$ is another negative maximum. This suggests that the degree of deviation from the adiabatic state, however small but finite, is important in forming the profiles of the zonal flow that is fast and negative and the turbulence. Another point to notice is that, where the zonal flow changes directions, $\sin\delta<0$ and $\beta<1$ by the time $t=2\times10^3$. It is checked that the feature holds up to $t=2\times10^4$.

In order to further examine the characteristics of the turbulence, the spectral distribution of $|\tilde{\varphi}_k|^2$ and δ_k at significant locations are shown in figure 5. Near $x=16$ the energy spectrum changes from being peaked near $k\ll1$ at $t=600$ to being broadly peaked around $1\leqslant k\leqslant2$ after the appearance of a sub-peak around $k\approx2$ at $t=800$ (*a*). By $t=2\times10^3$ the energy spectrum at $x=47$ similarly becomes broad in k, not sharply peaked at low k (*c*). Yet the spectrum at $x=30$ remains peaked

https://doi.org/10.1017/S0022377820000549 Published online by Cambridge University Press

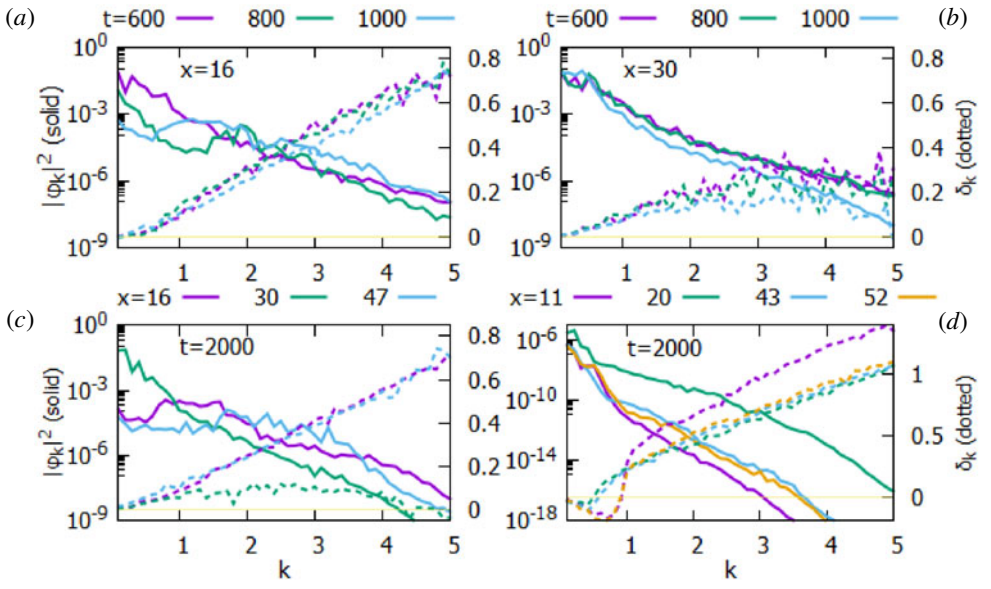


FIGURE 5. Spectrum and the cross-phase where the turbulence is either locally strong or weak: at $x = 16$ (a), where $\bar{V}$ is negative and large, and $x = 30$ (b) where $\bar{V}$ is positive and large, each averaged over a time interval $\Delta t = 200$ centred at $t = 6 \times 10^2$, 8×10^2 and 10^3, respectively. Spectra and the cross-phases at a quasi-steady state (averaged between $t = 1.8 \times 10^3$ and 2×10^3) where the turbulence level is locally strong (c) and negligibly weak (d).

near the lowest k (b,c). At all three locations δ_k is found to increase in terms of k. Since δ_k at $x = 30$ is smaller than at $x = 16$, the effective cross-phase at $x = 16$ and 47 is larger than at $x = 30$ (see figure 4). Also shown are the spectra at the locations of minimal fluctuation, $x = 11$, 20, 43 and 52, at $t = 2 \times 10^3$ (d). Albeit small, they are peaked at the lowest possible k and δ_k of $k \ll 1$ is found to be negative.

In figure 6 β_k values at $x = 16$ and 47 are larger than at $x = 30$, which are nearly 1 all over k. Also plotted in the figure is the spectral distribution of δ_{1k} obtained by the subtraction $\delta_k - \delta_{0k}$, which contains explicit contributions of $\bar{V}$ and $\bar{n}'$. At a quasi-steady state at $t = 2 \times 10^3$ it is found that δ_{1k} of the fluctuations at $x = 16$, 47 and 30 are all negative (c). This means that the zonal fields $\bar{V}$ and $\bar{n}'$ reduce the cross-phase around the peaks of $\bar{V}$. As a result the instability is tamed and the fluctuation level becomes lower. Since the fluctuation energy is concentrated in low-k modes at $x = 30$, such reduction of the cross-phase is not as relevant as at $x = 16$ and 47. It is clear that δ_k at the locations of minimal fluctuation is negative for $k < 1$ because of δ_k being negative (d).

In summary, for $\alpha = 5.0$, the fluctuations are limited around the peaks of the zonal flow that is generated dynamically by the non-zonal turbulence. Depending on the direction of the zonal flow, the fluctuations exhibit different characteristics: at a positive peak of $\bar{V}$ low-k fluctuations are strong whereas most energy is carried by the fluctuations of $1 \leqslant k \leqslant 2$ at a negative peak. As a result, the turbulence around the region of positive peak of $\bar{V}$ is present in a wider region than that of the negative peak of $\bar{V}$ if the fluctuations are not far from isotropic. Since the cross-phase increases with k, the fluctuations where $\bar{V}$ is a negative peak are effectively further away from being adiabatic than where $\bar{V}$ is a positive peak. In between the regions of fast $\bar{V}$

https://doi.org/10.1017/S0022377820000549 Published online by Cambridge University Press

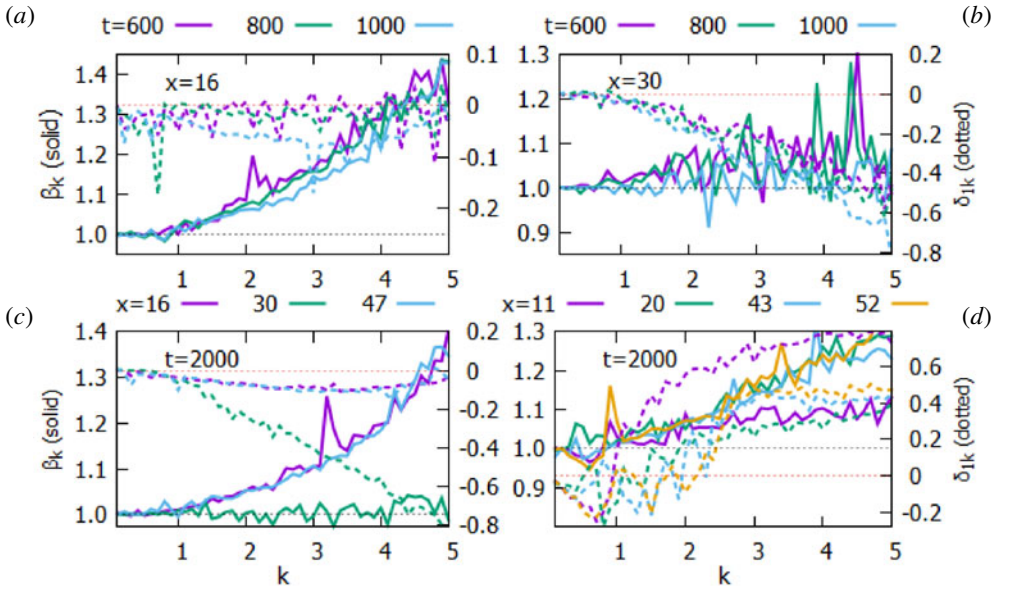


FIGURE 6. The ratio $\beta_k = |\tilde{n}_k|/|\tilde{\varphi}_k|$ and the cross-phase δ_{1k}, that is explicitly dependent on the zonal fields, where the turbulence is either locally strong or weak: at $x = 16$ (*a*), where $\bar{V}$ is negative and large, and $x = 30$ (*b*) where $\bar{V}$ is positive and large, each averaged over a time interval $\Delta t = 200$ centred at $t = 6 \times 10^2$, 8×10^2 and 10^3. $\beta_k = |\tilde{n}_k|/|\tilde{\varphi}_k|$ and δ_{1k} at a quasi-steady state (averaged between $t = 1.8 \times 10^3$ and 2×10^3) where the turbulence level is locally strong (*c*) and negligibly weak (*d*).

exist narrow layers of negligible fluctuations. They are formed by stabilization of the energetic fluctuations through the reductions of δ_k to be negative and of β_k below 1 by the zonal fields.

4. Conclusions

In the fusion experiments better plasma confinement (H mode) is achieved when the zonal flow is present at the edge region of the plasma. ZF is believed to serve in forming a narrow transport barrier, where the pressure gradient becomes steeper, than inside the plasma. Edge plasma of radial width $20\pi\rho_s$ is simulated numerically by the modified Hasegawa–Wakatani model of the electrostatic potential and the electron density. With the adiabaticity parameter $\alpha = 0.5$, 1.0 and 5.0 quasi-sinusoidal ZF $\bar{V}$ of amplitude approximately $2(\rho_s/L_n)c_s$ is generated self-consistently out of the non-zonal fluctuations. ZF kinetic energy is roughly 100 times larger than the non-zonal part in the steady state. For less adiabatic cases of $\alpha = 0.5$ and 1.0 turbulence is widespread and oscillating in time, not particularly trapped with the zonal flow. Highly adiabatic case of $\alpha = 5.0$, however, develops a localized turbulence pattern trapped within the zonal flow. The fluctuations are found to be localized away from the narrow regions where ZF changes the direction. Non-zonal potential is stable near $\bar{V} = 0$ because the resistive electron response along the parallel direction works as reducing rather than increasing the energy. At the same locations the non-zonal density is stable because the cross-phase between the potential and the density is negative due to large ZF gradient $\bar{V}'$. Density fluctuation also forms a strong zonal component $\bar{n}$. The zonal-density gradient $\bar{n}'$ is positive and large at the peak location of the turbulence

https://doi.org/10.1017/S0022377820000549 Published online by Cambridge University Press

while it is negative in the layer of $\bar{V} \approx 0$. Thus the overall density gradient including the background as well as the zonal part becomes steeper within the layer. Similar stabilization of the fluctuations near $\bar{V} = 0$ is observed in the model, which imposes a sinusoidal ZF of amplitude $2(\rho_s/L_n)c_s$, instead of allowing the ZF to be generated dynamically.

ZF turns out to work in many facets in its feedback to the turbulence: ZF can extract the energy from the turbulence with the rate proportional to $\bar{V}$ itself and the gradient of the Reynolds stress. Non-uniformity of ZF, $\bar{V}'$ and $\bar{V}''$, may further reduce the peak level of the turbulence by lowering the cross-phase.

Sufficiently large gradient of quasi-sinusoidal ZF around $\bar{V} = 0$ may develop a layer of negative cross-phase that impedes transport. In the layer ZF is negligibly slow and the non-zonal fluctuations are weak. As a result, the Reynolds stress and the triad interactions between non-zonal fluctuations cannot provide sufficient power to eclipse the resistive loss of the fluctuation kinetic energy. It is desirable to extend to the plasma turbulence model where the temperature is allowed to change by the heat flux. Work is still in progress to study the stabilization and the localization of the fluctuations in the fluid models of the ion-temperature-gradient turbulence and the electromagnetic resistive-drift turbulence.

Acknowledgements

This work is dedicated to Professor J. A. Krommes who inspired C.-B.K. and taught everything that C.-B.K. knows about the plasma turbulence. C.-B.K. acknowledges discussions with Professors M. Hole and R. Dewar of Australian National University during the visit in 2019. This work was supported by the Korea Research Foundation Grant funded by the Korean Government (NRF-2020R1F1A1072570). The numerical work was made possible by the Supercomputing Center/Korea Institute of Science and Technology Information with supercomputing resources including technical support (KSC-2019-CRE-0151).

REFERENCES

ARAKAWA, A. 1966 Computational design for long-term numerical integrations of the equations of atmospheric motion. *J. Comput. Phys.* **1**, 110.

BIGLARI, H., DIAMOND, P. H. & TERRY, P. W. 1990 Influence of sheared poloidal rotation on edge turbulence. *Phys. Fluids* B **2**, 1.

BIRKENMEIER, G., RAMISCH, M., SCHMID, B. & STROTH, U. 2013 Experimental evidence of turbulent transport regulation by zonal flows. *Phys. Rev. Lett.* **110**, 145004.

BURRELL, K. H. 1999 Tests of causality: experimental evidence that sheared $\boldsymbol{E} \times \boldsymbol{B}$ flow alters turbulence and transport in tokamaks. *Phys. Plasmas* **6**, 4418.

CARMARGO, S. J., TIPPETT, M. K. & CALDAS, I. L. 1998 Nonmodal energetics of resistive drift waves. *Phys. Rev.* E **58**, 3693.

DIAMOND, P. H., ITOH, S.-I., ITOH, K. & HAHM, T. S. 2005 Zonal flows in plasma – a review. *Plasma Phys. Control. Fusion* **47**, R35.

DUDSON, B. D., UMANSKY, M. V., XU, X. Q., SNYDER, P. B. & WILSON, H. R. 2009 Bout++: a framework for parallel plasma fluid simulations. *Comput. Phys. Commun.* **180**, 1467.

FIGARELLA, C. F., BENKADDA, S., BEYER, P., GARBET, X. & VOITSEKHOVITCH, I. 2003 Transport reduction by rotation shear in tokamak-edge turbulence. *Phys. Rev. Lett.* **90**, 015002.

FREETHY, S. J., GÖRLER, T., CREELY, A. J., CONWAY, G. D., DENK, S. S., HAPPEL, T., KOENEN, C., HENNEQUIN, P., WHITE, A. E. & ASDEX UPGRADE TEAM 2018 Validation of gyrokinetic simulations with measurements of electron temperature fluctuations and density–temperature phase angles on ASDEX upgrade. *Phys. Plasmas* **25**, 055903.

https://doi.org/10.1017/S0022377820000549 Published online by Cambridge University Press

FUJISAWA, A. 2009 A review of zonal flow experiments. *Nucl. Fusion* **49**, 013001.

GUTTENFELDER, W., KAYE, S. M., KRIETE, D. M., BELL, R. E., DIALLO, A., LEBLANC, B. P., MCKEE, G. R., PODESTA, M., SABBAGH, S. A. & SMITH, D. R. 2019 Initial transport and turbulence analysis and gyrokinetic simulation validation in NSTX-U L-mode plasmas. *Nucl. Fusion* **59**, 056027.

HASEGAWA, A. & WAKATANI, M. 1983 Plasma edge turbulence. *Phys. Rev. Lett.* **50**, 682.

HILLESHEIM, J. C., DELABIE, E., MEYER, H., MAGGI, C. F., MENESES, L., POLI, E. & JET CONTRIBUTORS 2016 Stationary zonal flows during the formation of the edge transport barrier in the jet tokamak. *Phys. Rev. Lett.* **116**, 065002.

HORTON, W. 1999 Drift waves and transport. *Rev. Mod. Phys.* **71**, 735.

KIM, C.-B., AN, C.-Y. & MIN, B. 2019*a* Reduction of edge plasma turbulence via cross-phase decrease by zonal fields. *Plasma Phys. Control. Fusion* **61** (8), 085024.

KIM, C.-B., MIN, B. & AN, C.-Y. 2018 Localization of the eigenmode of the drift-resistive plasma by zonal flow. *Phys. Plasmas* **25** (10), 102501.

KIM, C.-B., MIN, B. & AN, C.-Y. 2019*b* On the effects of nonuniform zonal flow in the resistive-drift plasma. *Plasma Phys. Control. Fusion* **61** (3), 035002.

KOBAYASHI, T., ITOH, K., IDO, T., KAMIYA, K., ITOH, S.-I., MIURA, Y., NAGASHIMA, Y., FUJISAWA, A., INAGAKI, S. & IDA, K. 2017 Turbulent transport reduction induced by transition on radial electric field shear and curvature through amplitude and cross-phase in torus plasma. *Sci. Rep.* **7**, 14971.

KROMMES, J. A. & KIM, C.-B. 2000 Interactions of disparate scales in drift-wave turbulence. *Phys. Rev.* E **62**, 8508.

MAKWANA, K. D., TERRY, P. W., PUESCHEL, M. J. & HATCH, D. R. 2014 Subdominant modes in zonal-flow-regulated turbulence. *Phys. Rev. Lett.* **112**, 095002.

NAULIN, V. & SPATSCHEK, K. H. 1997 Nonlinear drift-wave structures and their influence on particle transport. *Phys. Rev.* E **55**, 5883.

NUMATA, R., BALL, R. & DEWAR, R. L. 2007 Bifurcation in electrostatic resistive drift wave turbulence. *Phys. Plasmas* **14**, 102312.

ROSENBLUTH, M. N. & HINTON, F. L. 1998 Poloidal flow driven by ion-temperature-gradient turbulence in tokamaks. *Phys. Rev. Lett.* **80**, 724.

SCHAFFNER, D. A., CARTER, T. A., ROSSI, G. D., GUICE, D. S., MAGGS, J. E., VINCENA, S. & FRIEDMAN, B. 2012 Modification of turbulent transport with continuous variation of flow shear in the large plasma device. *Phys. Rev. Lett.* **109**, 135002.

SHAING, K. C. & CRUME, E. C. 1989 Bifurcation theory of poloidal rotation in tokamaks: a model for L–H transition. *Phys. Rev. Lett.* **63**, 2369.

SHCHEPETOV, S. V., KHOLNOV, YU. V. & VASIL'KOV, D. G. 2013 On the phase shift between electric potential and plasma density fluctuations in the edge turbulence. *Plasma Phys. Rep.* **39**, 130.

TERRY, P. W. 2000 Suppression of turbulence and transport by sheared flow. *Rev. Mod. Phys.* **72**, 109.

TERRY, P. W., NEWMAN, D. E. & WARE, A. S. 2001 Suppression of transport cross phase by strongly sheared flow. *Phys. Rev. Lett.* **87**, 185001.

TYNAN, G. R., FUJISAWA, A. & MCKEE, G. 2009 A review of experimental drift turbulence studies. *Plasma Phys. Control. Fusion* **51**, 113001.

WAGNER, F. 2018 The history of research into improved confinement. *Eur. Phys. J.* H **43**, 523.

WAGNER, F., BECKER, G., BEHRINGER, K., CAMPBELL, D., EBERHAGEN, A., ENGELHARDT, W., FUSSMANN, G., GEHRE, O., GERNHARDT, J., GIERKE, G. V. *et al.* 1982 Regime of improved confinement and high beta in neutral-beam-heated divertor discharges of the ASDEX tokamak. *Phys. Rev. Lett.* **49**, 1408.

WHITE, A. E., PEEBLES, W. A., RHODES, T. L., HOLLAND, C. H., WANG, G., SCHMITZ, L., CARTER, T. A., HILLESHEIM, J. C., DOYLE, E. J., ZENG, L. *et al.* 2010 Measurement of the cross-phase angle between density and electron temperature fluctuations and comparison with gyrokinetic simulations. *Phys. Plasmas* **17**, 056103.

https://doi.org/10.1017/S0022377820000549 Published online by Cambridge University Press